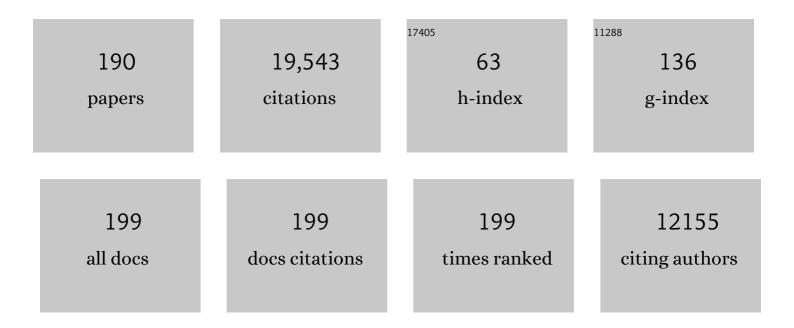
## David Sandwell

List of Publications by Year in descending order

Source: https://exaly.com/author-pdf/314708/publications.pdf Version: 2024-02-01



#	Article	IF	CITATIONS
1	Global Sea Floor Topography from Satellite Altimetry and Ship Depth Soundings. Science, 1997, 277, 1956-1962.	6.0	3,781
2	Marine gravity anomaly from Geosat and ERS 1 satellite altimetry. Journal of Geophysical Research, 1997, 102, 10039-10054.	3.3	1,505
3	Global Bathymetry and Elevation Data at 30 Arc Seconds Resolution: SRTM30_PLUS. Marine Geodesy, 2009, 32, 355-371.	0.9	1,168
4	New global marine gravity model from CryoSat-2 and Jason-1 reveals buried tectonic structure. Science, 2014, 346, 65-67.	6.0	1,074
5	Biharmonic spline interpolation of GEOSâ€3 and SEASAT altimeter data. Geophysical Research Letters, 1987, 14, 139-142.	1.5	602
6	Global marine gravity from retracked Geosat and ERSâ€l altimetry: Ridge segmentation versus spreading rate. Journal of Geophysical Research, 2009, 114, .	3.3	591
7	Global Bathymetry and Topography at 15ÂArcÂSec: SRTM15+. Earth and Space Science, 2019, 6, 1847-1864.	1.1	440
8	Bathymetric prediction from dense satellite altimetry and sparse shipboard bathymetry. Journal of Geophysical Research, 1994, 99, 21803-21824.	3.3	404
9	Three-dimensional deformation caused by the Bam, Iran, earthquake and the origin of shallow slip deficit. Nature, 2005, 435, 295-299.	13.7	403
10	Open radar interferometry software for mapping surface Deformation. Eos, 2011, 92, 234-234.	0.1	269
11	The Global Seamount Census. Oceanography, 2010, 23, 24-33.	0.5	262
12	Evolution of the eastern Indian Ocean since the Late Cretaceous: Constraints from Geosat altimetry. Journal of Geophysical Research, 1989, 94, 13755-13782.	3.3	254
13	Toward 1-mGal accuracy in global marine gravity from CryoSat-2, Envisat, and Jason-1. The Leading Edge, 2013, 32, 892-899.	0.4	208
14	Phase gradient approach to stacking interferograms. Journal of Geophysical Research, 1998, 103, 30183-30204.	3.3	203
15	Folding of oceanic lithosphere. Journal of Geophysical Research, 1985, 90, 8563-8569.	3.3	200
16	Tectonic history and new isochron chart of the south Pacific. Journal of Geophysical Research, 1990, 95, 8543-8567.	3.3	174
17	Lineâ€ofâ€sight displacement from ALOSâ€2 interferometry: <i>M<sub>w</sub></i> 7.8 Gorkha Earthquake and <i>M<sub>w</sub></i> 7.3 aftershock. Geophysical Research Letters, 2015, 42, 6655-6661.	1.5	174
18	Deformation on Nearby Faults Induced by the 1999 Hector Mine Earthquake. Science, 2002, 297, 1858-1862.	6.0	171

#	Article	IF	CITATIONS
19	Accuracy and resolution of shuttle radar topography mission data. Geophysical Research Letters, 2003, 30, .	1.5	170
20	Fault creep along the southern San Andreas from interferometric synthetic aperture radar, permanent scatterers, and stacking. Journal of Geophysical Research, 2003, 108, .	3.3	169
21	Highâ€resolution interseismic velocity data along the San Andreas Fault from GPS and InSAR. Journal of Geophysical Research: Solid Earth, 2013, 118, 369-389.	1.4	139
22	Evidence for diffuse extension of the Pacific Plate from Pukapuka ridges and cross-grain gravity lineations. Journal of Geophysical Research, 1995, 100, 15087-15099.	3.3	137
23	Crustal volumes of the continents and of oceanic and continental submarine plateaus. Earth and Planetary Science Letters, 1989, 92, 234-246.	1.8	136
24	Accuracy and Resolution of ALOS Interferometry: Vector Deformation Maps of the Father's Day Intrusion at Kilauea. IEEE Transactions on Geoscience and Remote Sensing, 2008, 46, 3524-3534.	2.7	135
25	Antarctic marine gravity field from high-density satellite altimetry. Geophysical Journal International, 1992, 109, 437-448.	1.0	119
26	Retracking ERS-1 altimeter waveforms for optimal gravity field recovery. Geophysical Journal International, 2005, 163, 79-89.	1.0	117
27	The 2010 Maule, Chile earthquake: Downdip rupture limit revealed by space geodesy. Geophysical Research Letters, 2010, 37, .	1.5	117
28	Lithospheric flexure at fracture zones. Journal of Geophysical Research, 1982, 87, 4657-4667.	3.3	114
29	Coseismic slip model of the 2008 Wenchuan earthquake derived from joint inversion of interferometric synthetic aperture radar, GPS, and field data. Journal of Geophysical Research, 2010, 115, .	3.3	111
30	Geoid height versus topography for oceanic plateaus and swells. Journal of Geophysical Research, 1989, 94, 7403-7418.	3.3	110
31	A detailed view of the South Pacific geoid from satellite altimetry. Journal of Geophysical Research, 1984, 89, 1089-1104.	3.3	106
32	The lowest place on Earth is subsiding—An InSAR (interferometric synthetic aperture radar) perspective. Bulletin of the Geological Society of America, 2002, 114, 12-23.	1.6	102
33	Decorrelation of L-Band and C-Band Interferometry Over Vegetated Areas in California. IEEE Transactions on Geoscience and Remote Sensing, 2010, 48, 2942-2952.	2.7	101
34	Thermal stress and the spacings of transform faults. Journal of Geophysical Research, 1986, 91, 6405-6417.	3.3	100
35	Thermomechanical evolution of oceanic fracture zones. Journal of Geophysical Research, 1984, 89, 11401-11413.	3.3	99
36	Flexural ridges, trenches, and outer rises around coronae on Venus. Journal of Geophysical Research, 1992, 97, 16069-16083.	3.3	97

#	Article	IF	CITATIONS
37	Retracking CryoSat-2, Envisat and Jason-1 radar altimetry waveforms for improved gravity field recovery. Geophysical Journal International, 2014, 196, 1402-1422.	1.0	97
38	Refining the shallow slip deficit. Geophysical Journal International, 2016, 204, 1843-1862.	1.0	95
39	Satellite interferometric observations of displacements associated with seasonal groundwater in the Los Angeles basin. Journal of Geophysical Research, 2002, 107, ETG 8-1-ETG 8-15.	3.3	94
40	Evidence from en-echelon cross-grain ridges for tensional cracks in the Pacific plate. Nature, 1987, 329, 534-537.	13.7	92
41	Evidence for Retrograde Lithospheric Subduction on Venus. Science, 1992, 257, 766-770.	6.0	92
42	Locking depths estimated from geodesy and seismology along the San Andreas Fault System: Implications for seismic moment release. Journal of Geophysical Research, 2011, 116, .	3.3	91
43	Geoid height versus age for symmetric spreading ridges. Journal of Geophysical Research, 1980, 85, 7235-7241.	3.3	89
44	Compensation of swells and plateaus in the north Pacific: No direct evidence for mantle convection. Journal of Geophysical Research, 1988, 93, 2775-2783.	3.3	89
45	Tectonic and Anthropogenic Deformation at the Cerro Prieto Geothermal Step-Over Revealed by Sentinel-1A InSAR. IEEE Transactions on Geoscience and Remote Sensing, 2017, 55, 5284-5292.	2.7	89
46	Lithospheric bending at subduction zones based on depth soundings and satellite gravity. Journal of Geophysical Research, 1995, 100, 379-400.	3.3	86
47	Interseismic deformation and creep along the central section of the North Anatolian Fault (Turkey): InSAR observations and implications for rateâ€andâ€state friction properties. Journal of Geophysical Research: Solid Earth, 2013, 118, 316-331.	1.4	85
48	Features on Venus generated by plate boundary processes. Journal of Geophysical Research, 1992, 97, 13533-13544.	3.3	82
49	Localized and distributed creep along the southern San Andreas Fault. Journal of Geophysical Research: Solid Earth, 2014, 119, 7909-7922.	1.4	82
50	An abrupt change in ridge axis gravity with spreading rate. Journal of Geophysical Research, 1989, 94, 17383-17392.	3.3	81
51	Gravity field recovery from geodetic altimeter missions. Advances in Space Research, 2021, 68, 1059-1072.	1.2	80
52	Global gravity, bathymetry, and the distribution of submarine volcanism through space and time. Journal of Geophysical Research, 2006, 111, .	3.3	78
53	Coseismic Displacements and Surface Fractures from Sentinel-1 InSAR: 2019 Ridgecrest Earthquakes. Seismological Research Letters, 2020, 91, 1979-1985.	0.8	78
54	Geoid heightâ€age relation from SEASAT altimeter profiles across the Mendocino Fracture Zone. Journal of Geophysical Research, 1982, 87, 3949-3958.	3.3	73

#	Article	IF	CITATIONS
55	The 1999 (Mw 7.1) Hector Mine, California, Earthquake: Near-Field Postseismic Deformation from ERS Interferometry. Bulletin of the Seismological Society of America, 2002, 92, 1433-1442.	1.1	73
56	A Clobal Survey of Possible Subduction Sites on Venus. Icarus, 1995, 117, 173-196.	1.1	69
57	Upper-plate controls on co-seismic slip in the 2011 magnitude 9.0 Tohoku-oki earthquake. Nature, 2016, 531, 92-96.	13.7	69
58	Warping and cracking of the Pacific plate by thermal contraction. Journal of Geophysical Research, 2004, 109, .	3.3	68
59	Slip on faults in the Imperial Valley triggered by the 4 April 2010 Mw 7.2 El Mayor-Cucapah earthquake revealed by InSAR. Geophysical Research Letters, 2011, 38, n/a-n/a.	1.5	68
60	The negative gravity field over the 85°E ridge. Journal of Geophysical Research, 1982, 87, 7673-7686.	3.3	67
61	Global distribution of seamounts from Seasat profiles. Journal of Geophysical Research, 1988, 93, 10408-10420.	3.3	66
62	Small-scale deformations associated with the 1992 Landers, California, earthquake mapped by synthetic aperture radar interferometry phase gradients. Journal of Geophysical Research, 1998, 103, 27001-27016.	3.3	66
63	A model of the earthquake cycle along the San Andreas Fault System for the past 1000 years. Journal of Geophysical Research, 2006, 111, .	3.3	66
64	El Mayor-Cucapah ( <i>M<sub>w</sub></i> 7.2) earthquake: Early near-field postseismic deformation from InSAR and GPS observations. Journal of Geophysical Research: Solid Earth, 2014, 119, 1482-1497.	1.4	66
65	Is there a discrepancy between geological and geodetic slip rates along the San Andreas Fault System?. Journal of Geophysical Research: Solid Earth, 2014, 119, 2518-2538.	1.4	65
66	Global mesoscale variability from the Geosat Exact Repeat Mission: Correlation with ocean depth. Journal of Geophysical Research, 1989, 94, 17971-17984.	3.3	64
67	Coulomb stress accumulation along the San Andreas Fault system. Journal of Geophysical Research, 2003, 108, .	3.3	64
68	Optimal combination of InSAR and GPS for measuring interseismic crustal deformation. Advances in Space Research, 2010, 46, 236-249.	1.2	64
69	Marine gravity of the southern ocean and Antarctic margin from Geosat. Journal of Geophysical Research, 1988, 93, 10389-10396.	3.3	63
70	Highâ€accuracy, highâ€resolution gravity profiles from 2 years of the Geosat Exact Repeat Mission. Journal of Geophysical Research, 1990, 95, 3049-3060.	3.3	59
71	Lithospheric flexure on Venus. Geophysical Journal International, 1994, 119, 627-647.	1.0	59
72	Seamount Discovery Tool Aids Navigation to Uncharted Seafloor Features. Oceanography, 2010, 23, 34-36.	0.5	59

#	Article	IF	CITATIONS
73	Variations of global mesoscale eddy energy observed from Geosat. Journal of Geophysical Research, 1990, 95, 17865-17876.	3.3	58
74	Systematics of ridge propagation south of 30°S. Earth and Planetary Science Letters, 1994, 121, 245-258.	1.8	58
75	Tectonic fabric map of the ocean basins from satellite altimetry data. Tectonophysics, 1988, 155, 1-26.	0.9	57
76	Near real-time radar interferometry of the Mw 7.1 Hector Mine Earthquake. Geophysical Research Letters, 2000, 27, 3101-3104.	1.5	56
77	Magmatically Triggered Slow Slip at Kilauea Volcano, Hawaii. Science, 2008, 321, 1177-1177.	6.0	55
78	Ocean loading effects on stress at near shore plate boundary fault systems. Journal of Geophysical Research, 2010, 115, .	3.3	54
79	Conventional Bathymetry, Bathymetry from Space, and Geodetic Altimetry. Oceanography, 2004, 17, 8-23.	0.5	53
80	An analysis of ridge axis gravity roughness and spreading rate. Journal of Geophysical Research, 1992, 97, 3235-3245.	3.3	50
81	Bathymetry from space: Rationale and requirements for a new, high-resolution altimetric mission. Comptes Rendus - Geoscience, 2006, 338, 1049-1062.	0.4	50
82	Three-dimensional models of elastostatic deformation in heterogeneous media, with applications to the Eastern California Shear Zone. Geophysical Journal International, 2009, 179, 500-520.	1.0	50
83	Driving Forces for Limited Tectonics on Venus. Icarus, 1997, 129, 232-244.	1.1	49
84	A silent <i>M</i> <sub><i>w</i></sub> 4.7 slip event of October 2006 on the Superstition Hills fault, southern California. Journal of Geophysical Research, 2009, 114, .	3.3	49
85	Thermal isostasy: Response of a moving lithosphere to a distributed heat source. Journal of Geophysical Research, 1982, 87, 1001-1014.	3.3	47
86	Comparison of marine gravity from shipboard and highâ€density satellite altimetry along the Midâ€Atlantic Ridge, 30.5°–35.5°S. Geophysical Research Letters, 1993, 20, 1639-1642.	1.5	47
87	A three-dimensional semianalytic viscoelastic model for time-dependent analyses of the earthquake cycle. Journal of Geophysical Research, 2004, 109, .	3.3	47
88	Documentation of Surface Fault Rupture and Ground-Deformation Features Produced by the 4 and 5 July 2019 MwÂ6.4 and MwÂ7.1 Ridgecrest Earthquake Sequence. Seismological Research Letters, 2020, 91, 2942-2959.	0.8	47
89	Coseismic deformation associated with the November 1995,MW= 7.1 Nuweiba earthquake, Gulf of Elat (Aqaba), detected by synthetic aperture radar interferometry. Journal of Geophysical Research, 1999, 104, 25221-25232.	3.3	46
90	Estimates of stress drop and crustal tectonic stress from the 27 February 2010 Maule, Chile, earthquake: Implications for fault strength. Journal of Geophysical Research, 2011, 116, n/a-n/a.	3.3	46

#	Article	IF	CITATIONS
91	Slow Slip Event On the Southern San Andreas Fault Triggered by the 2017 <i>M</i> <sub><i>w</i></sub> 8.2 Chiapas (Mexico) Earthquake. Journal of Geophysical Research: Solid Earth, 2019, 124, 9956-9975.	1.4	46
92	Comparison of along-track resolution of stacked Geosat, ERS 1, and TOPEX satellite altimeters. Journal of Geophysical Research, 1995, 100, 15117-15127.	3.3	45
93	Global correlation of mesoscale ocean variability with seafloor roughness from satellite altimetry. Geophysical Research Letters, 2000, 27, 1251-1254.	1.5	44
94	Inversion of marine gravity anomalies over southeastern China seas from multi-satellite altimeter vertical deflections. Journal of Applied Geophysics, 2017, 137, 128-137.	0.9	42
95	The GPlates Portal: Cloud-Based Interactive 3D Visualization of Global Geophysical and Geological Data in a Web Browser. PLoS ONE, 2016, 11, e0150883.	1.1	41
96	Surface deformation associated with fractures near the 2019 Ridgecrest earthquake sequence. Science, 2020, 370, 605-608.	6.0	41
97	Interpolation of 2â€D vector data using constraints from elasticity. Geophysical Research Letters, 2016, 43, 10,703.	1.5	40
98	Diffuse interseismic deformation across the Pacific–North America plate boundary. Geology, 2007, 35, 311.	2.0	39
99	Deformation-related volcanism in the Pacific Ocean linked to the Hawaiian–Emperor bend. Nature Geoscience, 2015, 8, 393-397.	5.4	38
100	Stress evolution of the San Andreas fault system: Recurrence interval versus locking depth. Geophysical Research Letters, 2009, 36, .	1.5	37
101	Creep along the Imperial Fault, southern California, from GPS measurements. Journal of Geophysical Research, 2002, 107, ETG 12-1-ETG 12-13.	3.3	36
102	Observing global ocean circulation with SEASAT altimeter data. Marine Geodesy, 1984, 8, 67-83.	0.9	35
103	A preliminary tectonic fabric chart of the Indian Ocean. Journal of Earth System Science, 1989, 98, 7-24.	0.6	35
104	Topographic phase recovery from stacked ERS interferometry and a low-resolution digital elevation model. Journal of Geophysical Research, 2000, 105, 28211-28222.	3.3	35
105	Analysis of geoid height versus topography for oceanic plateaus and swells using nonbiased linear regression. Journal of Geophysical Research, 1991, 96, 8045-8055.	3.3	34
106	Modulation of the earthquake cycle at the southern San Andreas fault by lake loading. Journal of Geophysical Research, 2007, 112, .	3.3	34
107	Estimates of heat flow from Cenozoic seafloor using global depth and age data. Tectonophysics, 2006, 417, 325-335.	0.9	33
108	Gravity over Coronae and Chasmata on Venus. Icarus, 1994, 112, 130-146.	1.1	32

7

#	Article	IF	CITATIONS
109	Three-dimensional estimation of elastic thickness under the Louisville Ridge. Journal of Geophysical Research, 2000, 105, 13239-13252.	3.3	32
110	Retracking of SARAL/AltiKa Radar Altimetry Waveforms for Optimal Gravity Field Recovery. Marine Geodesy, 2017, 40, 40-56.	0.9	32
111	Mantle downwelling beneath the Australian-Antarctic discordance zone: evidence from geoid height versus topography. Earth and Planetary Science Letters, 1991, 103, 325-338.	1.8	31
112	Geodetic investigation into the deformation of the Salton Trough. Journal of Geophysical Research: Solid Earth, 2013, 118, 5030-5039.	1.4	31
113	On the source of crossâ€grain lineations in the central Pacific gravity field. Journal of Geophysical Research, 1989, 94, 9341-9352.	3.3	30
114	Joints in Venusian lava flows. Journal of Geophysical Research, 1992, 97, 13601-13610.	3.3	30
115	Vertical crustal displacement due to interseismic deformation along the San Andreas fault: Constraints from tide gauges. Geophysical Research Letters, 2014, 41, 3793-3801.	1.5	29
116	A compensation mechanism for the central Pacific. Journal of Geophysical Research, 1980, 85, 3751-3758.	3.3	27
117	What are the limitations of satellite altimetry?. The Leading Edge, 1998, 17, 73-76.	0.4	27
118	Chapter 12 Bathymetric Estimation. International Geophysics, 2001, , 441-xxxiv.	0.6	27
119	Oceanic microplate formation records the onset of India–Eurasia collision. Earth and Planetary Science Letters, 2016, 433, 204-214.	1.8	27
120	Seasonal variation in wind speed and sea state from global satellite measurements. Journal of Geophysical Research, 1984, 89, 2041-2051.	3.3	26
121	Geophysical Applications of Satellite Altimetry. Reviews of Geophysics, 1991, 29, 132-137.	9.0	26
122	Toward Absolute Phase Change Recovery With InSAR: Correcting for Earth Tides and Phase Unwrapping Ambiguities. IEEE Transactions on Geoscience and Remote Sensing, 2020, 58, 726-733.	2.7	26
123	Integrated Sentinelâ€1 InSAR and GNSS Timeâ€Series Along the San Andreas Fault System. Journal of Geophysical Research: Solid Earth, 2021, 126, e2021JB022579.	1.4	26
124	Transient Deformation in California From Two Decades of GPS Displacements: Implications for a Threeâ€Dimensional Kinematic Reference Frame. Journal of Geophysical Research: Solid Earth, 2019, 124, 12189-12223.	1.4	25
125	Outer trench slope flexure and faulting at Pacific basin subduction zones. Geophysical Journal International, 2019, 218, 708-728.	1.0	25
126	Global nondynamic orbit improvement for altimetric satellites. Journal of Geophysical Research, 1986, 91, 9447-9451.	3.3	24

#	Article	IF	CITATIONS
127	Imaging mid-ocean ridge transitions with satellite gravity. Geology, 1994, 22, 123.	2.0	24
128	Evolution of errors in the altimetric bathymetry model used by Google Earth and GEBCO. Marine Geophysical Researches, 2010, 31, 223-238.	0.5	22
129	The SARAL/AltiKa mission: A step forward to the future of altimetry. Advances in Space Research, 2021, 68, 808-828.	1.2	21
130	A contraction model for the flattening and equatorial ridge of lapetus. Icarus, 2010, 210, 817-822.	1.1	19
131	Appendix 1 : Indian Ocean Plate Reconstructions Since the Late Jurassic. Geophysical Monograph Series, 0, , 471-475.	0.1	19
132	Did stresses from the Cerro Prieto Geothermal Field influence the El Mayor ucapah rupture sequence?. Geophysical Research Letters, 2014, 41, 8767-8774.	1.5	19
133	The vertical fingerprint of earthquake cycle loading in southern California. Nature Geoscience, 2016, 9, 611-614.	5.4	19
134	Improved Bathymetric Prediction Using Geological Information: SYNBATH. Earth and Space Science, 2022, 9, .	1.1	19
135	A comparison of satellite and shipboard gravity measurements in the Gulf of Mexico. Geophysics, 1992, 57, 885-893.	1.4	18
136	The 1999 Hector Mine Earthquake, Southern California: Vector Near-Field Displacements from ERS InSAR. Bulletin of the Seismological Society of America, 2002, 92, 1341-1354.	1.1	18
137	Global estimates of seafloor slope from singleâ€beam ship soundings. Journal of Geophysical Research, 2008, 113, .	3.3	18
138	Slope correction for ocean radar altimetry. Journal of Geodesy, 2014, 88, 765-771.	1.6	18
139	An iterative spectral solution method for thin elastic plate flexure with variable rigidity. Geophysical Journal International, 2015, 200, 1012-1028.	1.0	18
140	Surface Creep Rate and Moment Accumulation Rate Along the Aceh Segment of the Sumatran Fault From Lâ€band ALOSâ€1/PALSARâ€1 Observations. Geophysical Research Letters, 2018, 45, 3404-3412.	1.5	18
141	GEOSAT GM data reveal new details of ocean floor. Eos, 1991, 72, 145-145.	0.1	17
142	Modal depth anomalies from multibeam bathymetry: Is there a South Pacific superswell?. Earth and Planetary Science Letters, 1996, 139, 1-16.	1.8	17
143	Bathymetry from space is now possible. Eos, 2003, 84, 37-44.	0.1	17
144	SAR interferometry at Venus for topography and change detection. Planetary and Space Science, 2012, 73, 130-144.	0.9	16

#	Article	IF	CITATIONS
145	Surface Creep Rate of the Southern San Andreas Fault Modulated by Stress Perturbations From Nearby Large Events. Geophysical Research Letters, 2018, 45, 10,259.	1.5	16
146	Seafloor geodesy from repeated sidescan sonar surveys. Journal of Geophysical Research: Solid Earth, 2016, 121, 4800-4813.	1.4	15
147	Kinematic Post-processing of Ship Navigation Data Using Precise Point Positioning. Journal of Navigation, 2019, 72, 795-804.	1.0	15
148	Synthetic Aperture Radar for Geodesy. Science, 1996, 273, 1181-1182.	6.0	14
149	Using InSAR to detect active deformation associated with faults in Suban field, South Sumatra Basin, Indonesia. The Leading Edge, 2014, 33, 882-888.	0.4	14
150	Improved Arctic Ocean Bathymetry Derived From DTU17 Gravity Model. Earth and Space Science, 2019, 6, 1336-1347.	1.1	14
151	Inflation along Kilauea's Southwest Rift Zone in 2006. Journal of Volcanology and Geothermal Research, 2008, 177, 418-424.	0.8	13
152	InSAR decorrelation to assess and prevent volcanic risk. European Journal of Remote Sensing, 2014, 47, 537-556.	1.7	13
153	The Unique Role of the Jason Geodetic Missions for high Resolution Gravity Field and Mean Sea Surface Modelling. Remote Sensing, 2021, 13, 646.	1.8	13
154	Stacked global satellite gravity profiles. Geophysics, 1999, 64, 1748-1755.	1.4	12
155	Applications of satellite altimetry to oceanography and geophysics. Marine Geophysical Researches, 1984, 7, 17-32.	0.5	11
156	Fracture zone traces across the north Pacific cretaceous quiet zone and their tectonic implications. Geophysical Monograph Series, 1993, , 137-154.	0.1	11
157	Constraints on 3â€D stress in the crust from support of midâ€ocean ridge topography. Journal of Geophysical Research, 2012, 117, .	3.3	11
158	An integral method to estimate the moment accumulation rate on the Creeping Section of the San Andreas Fault. Geophysical Journal International, 2015, 203, 48-62.	1.0	11
159	Comparison and evaluation of high-resolution marine gravity recovery via sea surface heights or sea surface siopes. Journal of Geodesy, 2021, 95, 1.	1.6	11
160	Along-track gravity anomalies from Geostat and Seasat altimetry: GEBCO overlays. Marine Geophysical Researches, 1992, 14, 165-205.	0.5	10
161	The Kara/Ust-Kara twin impact structure; A large-scale impact event in the Late Cretaceous. Special Paper of the Geological Society of America, 1990, , 233-238.	0.5	9
162	Radar interferometry for measuring tidal strains across cracks on Europa. Journal of Geophysical Research, 2004, 109, .	3.3	9

#	Article	IF	CITATIONS
163	Marine Vertical Gravity Gradients Reveal the Global Distribution and Tectonic Significance of "Seesaw―Ridge Propagation. Journal of Geophysical Research: Solid Earth, 2021, 126, e2020JB020017.	1.4	9
164	Significant improvements in marine gravity from ongoing satellite missions. Marine Geophysical Researches, 2013, 34, 137-146.	0.5	8
165	Interseismic Velocity Field and Seismic Moment Release in Northern Baja California, Mexico. Seismological Research Letters, 2018, 89, 526-533.	0.8	8
166	Assessment of ICESat-2 for the recovery of ocean topography. Geophysical Journal International, 2021, 226, 456-467.	1.0	7
167	On the Development of SWOT In Situ Calibration/Validation for Short-Wavelength Ocean Topography. Journal of Atmospheric and Oceanic Technology, 2022, 39, 595-617.	0.5	7
168	Global tectonic maps. , 2005, , .		5
169	GNSS-corrected InSAR displacement time-series spanning the 2019 Ridgecrest, CA earthquakes. Geophysical Journal International, 2022, 230, 1358-1373.	1.0	5
170	The Gravsat signal over tectonic features. Journal of Geophysical Research, 1984, 89, 4419-4426.	3.3	4
171	Marine gravity. Eos, 1988, 69, 1569.	0.1	4
172	Applications of Satellite Altimetry to Oceanography and Geophysics. , 1984, , 17-32.		4
173	A spectral expansion approach for geodetic slip inversion: implications for the downdip rupture limits of oceanic and continental megathrust earthquakes. Geophysical Journal International, 2018, 212, 400-411.	1.0	3
174	The Visualization Center at Scripps Institution of Oceanography: Education and Outreach. Seismological Research Letters, 2003, 74, 641-648.	0.8	2
175	Abyss-Lite: A High-resolution Gravimetric and Bathymetric Mission. , 2004, , .		2
176	Combining GPS and Remotely Sensed Data to Characterize Timeâ€Varying Crustal Motion. Eos, 2013, 94, 309-309.	0.1	2
177	Maxwell: A semi-analytic 4D code for earthquake cycle modeling of transform fault systems. Computers and Geosciences, 2018, 114, 84-97.	2.0	2
178	Meter-Scale Seafloor Geodetic Measurements Obtained from Repeated Multibeam Sidescan Surveys. Marine Geodesy, 2019, 42, 491-506.	0.9	2
179	Seismic Moment Accumulation Response to Lateral Crustal Variations of the San Andreas Fault System. Journal of Geophysical Research: Solid Earth, 2021, 126, e2020JB021208.	1.4	2
180	Marine Gravity from Satellite Altimetry over Ocean and Sea Ice. International Association of Geodesy Symposia, 1996, , 12-19.	0.2	2

#	Article	IF	CITATIONS
181	A Tectonic Chart for the Southern Ocean Derived from Geosat Altimetry Data. , 1990, , .		2
182	Reply to comment on: "Estimates of heat flow from Cenozoic seafloor using global depth and age data― Tectonophysics, 2006, 428, 101-103.	0.9	1
183	Physical principles of remote sensing: third edition. Geophysical Journal International, 2013, 195, 2050-2050.	1.0	1
184	A Comparison Between Satellite Gravity Data (Geosat) and Marine Gravity Data Measured in the Weddell Sea, Antarctica. International Association of Geodesy Symposia, 1992, , 129-138.	0.2	1
185	Reply [to "Comment on â€~Seasonal variation in wind speed and sea state from global satellite measurements' by D. Sandwell and R. Agreenâ€]. Journal of Geophysical Research, 1985, 90, 5009-5010.	3.3	Ο
186	Chapter 3 long term dynamics of the solid earth. , 1989, , 43-102.		0
187	Near-Field Deformation of the Imperial Valley, Southern California, from GPS and InSAR Measurements. International Association of Geodesy Symposia, 2002, , 506-511.	0.2	Ο
188	Plate Tectonics: A Martian View. , 2018, , 331-345.		0
189	INITIAL GEODETIC RESULTS FROM THE RESPONSE TO THE RIDGECREST EARTHQUAKE SEQUENCE. , 2019, , .		0
190	Vertical Postseismic Deformation of the 2019 Ridgecrest Earthquake Sequence. Journal of Geophysical Research: Solid Earth, 0, , .	1.4	0